Voltage-Gated Rearrangements Associated with Differential β-Subunit Modulation of the L-Type Ca^{2+} Channel Inactivation

Evgeny Kobrinsky,* Klaus J. F. Kepplinger,† Alexander Yu,* Jo Beth Harry,* Heike Kahr,† Christoph Romanin,† Darrell R. Abernethy,* and Nikolai M. Soldatov*

*National Institute on Aging, National Institutes of Health, Baltimore, Maryland 21224 USA; and †Institute for Biophysics, University of Linz, A-4040 Linz, Austria

ABSTRACT Auxiliary β-subunits bound to the cytoplasmic α_1-interaction domain of the pore-forming α_{1C}-subunit are important modulators of voltage-gated Ca^{2+} channels. The underlying mechanisms are not yet well understood. We investigated correlations between differential modulation of inactivation by β_{1a}- and β_2- subunits and structural responses of the channel to transition into distinct functional states. The NH_2-termini of the α_{1C}- and β-subunits were fused with cyan or yellow fluorescent proteins, and functionally coexpressed in COS1 cells. Fluorescence resonance energy transfer (FRET) between them or with membrane-trapped probes was measured in live cells under voltage clamp. It was found that in the resting state, the tagged NH_2-termini of the α_{1C}- and β-subunit fluorophores are separated. Voltage-dependent inactivation generates strong FRET between α_{1C} and β_{1a} suggesting mutual reorientation of the NH_2-termini, but their distance vis-à-vis the plasma membrane is not appreciably changed. These voltage-gated rearrangements were substantially reduced when the β_{1a}-subunit was replaced by β_2. Differential β-subunit modulation of inactivation and of FRET between α_{1C} and β were eliminated by inhibition of the slow inactivation. Thus, differential β-subunit modulation of inactivation correlates with the voltage-gated motion between the NH_2-termini of α_{1C}- and β-subunits and targets the mechanism of slow voltage-dependent inactivation.

INTRODUCTION

Calcium channels respond to membrane depolarization with an increase in membrane permeability that develops within a few milliseconds and then spontaneously decreases (inactivates) with characteristic kinetics. In the case of the L-type class C voltage-sensitive Ca^{2+} channel ($Ca_v1.2$), the replacement of Ca^{2+} with Ba^{2+} ions as the charge carrier eliminates Ca^{2+}-induced inactivation, and the Ba^{2+} current inactivates essentially in a voltage-dependent manner. Given the critical role of $Ca_v1.2$ channels in cell signaling (Soldatov, 2003), investigation of molecular correlates of inactivation has been an objective of a number of laboratories, including those cited in this article.

The $Ca_v1.2$ channel is composed of the pore-forming α_{1C}-subunit and the auxiliary β- and $\alpha_2\delta$-subunits. All three subunits can be colocalized along the plasma membrane in transfected cells expressing the functional recombinant channel (Gao et al., 1999). The subunits remain associated with each other after solubilization of the channel protein complex in mild nonionic detergents (Chang and Hosey, 1988) suggesting close association between the subunits in vivo. In fact, binding motifs involved in interactions between the α_{1C}- and β-subunits (Pragnell et al., 1994) as well as between the α_{1C}- and $\alpha_2\delta$-subunits (Gurnett and Campbell, 1996) have been identified.

The β-subunits are important modulators of the Ca^{2+} channel activity (Birnbaumer et al., 1998; Yamaguchi et al., 1998; Colecraft et al., 2002; Hullin et al., 2003; Takahashi et al., 2003). They are located on the cytoplasmic side of plasma membrane and generate the molecular signal necessary for correct plasma membrane targeting of the functional $Ca_v1.2$ complexes. Each of the four identified different types of β-subunit (β_1–β_4) binds, via the NH_2-terminal part of the second common conserved region (amino acids 262–290 in β_{1a} and 215–243 in β_{2a}), to the α_1-interaction domain (AID), a conserved motif in the cytoplasmic linker between repeats I and II of the α_1-subunit (Pragnell et al., 1994; De Waard et al., 1994). This binding was shown to be a molecular correlate for the well-established effect of β-subunits on the kinetics of $Ca_v1.2$ channel gating (Singer et al., 1991). Inactivation of the $Ca_v1.2$ channel is accelerated by the replacement of β_2 with the β_{1a}-subunit. The modulatory effect of the β-subunit was observed in other types of Ca^{2+} channels as well (Hummer et al., 2003). For example, in $Ca_v2.1$ (α_{1A}) P/Q-type channel, De Waard and Campbell (1995) identified β_{2a} as the least potent among four other types of β-subunit in acceleration of inactivation. Thus, β-subunits modulate both the functional expression and the gating of ion conductance.

Recently we have developed a new method for measuring dynamic structural responses to changes in the cell membrane potential (Kobrinsky et al., 2003). Using measurements of fluorescence resonance energy transfer (FRET) between enhanced cyan (ECFP) and yellow (EYFP) fluorescent proteins under voltage-clamp conditions in live cells, we provided evidence that ECFP/EYFP-tagged

Submitted February 4, 2004, and accepted for publication April 20, 2004.

Address reprints requests to N. M. Soldatov, National Institute on Aging, National Institutes of Health, 5600 Nathan Shock Dr., Baltimore, MD 21224. Tel.: 410-558-8343; Fax: 410-558-8318; E-mail: soldatovN@grc.nia.nih.gov.

0006-3495/04/08/844/14 $2.00

doi: 10.1529/biophysj.104.041152

cytoplasmic tails of the $Ca_v1.2$ channel are moving parts, responsive to voltage gating. The voltage-dependent mobility of the COOH-terminal tail was found to be essential for Ca^{2+}-dependent inactivation and Ca^{2+} signal transduction.

Here we have applied FRET imaging in voltage-clamped living COS1 cells to directly compare the interaction between α_{1C} and different β-subunits in different functional states of the channel, and to determine molecular motions of the β-subunits vis-à-vis α_{1C} and the plasma membrane. Two pore-forming α_{1C}-subunits showing different inactivation properties were used. The $\alpha_{1C,77}$-subunit has the structure of the most common α_{1C} splice variant and thus can be referred to as the ''wild-type'' isoform. The $\alpha_{1C,IS\text{-}IV}$-subunit gives rise to a channel that does not show the slow voltage-dependent inactivation (Shi and Soldatov, 2002). This isoform was generated by the mutation of the following four amino acids in the transmembrane segments S6 of the $\alpha_{1C,77}$-subunit: S405I in IS6, A752T in IIS6, V1165T in IIIS6, and I1475T in IVS6. These mutations are located in positions −1 (IS6) and −2 (IIS6–IVS6) and thus form a ring of altered amino acid residues at the inner mouth of the pore. The corresponding structure in the $\alpha_{1C,77}$ channel was named the ''annular determinant of slow inactivation'' (ADSI) reflecting the specific arrangement of crucial amino acids with regards to the ion-conducting pore.

The β-subunit variants β_{1a}, cloned from rabbit skeletal muscle (Mori et al., 1991), and β_2, originally cloned from rabbit heart (Hullin et al., 1992), have been studied in this work as modulators of Ca^{2+} channel inactivation. The rabbit β_2-subunit has 92.6% overall amino acid identity to the rat β_{2a} protein (Perez-Reyes et al., 1992) with some variations (17 amino acids) at the NH_2-terminus, and lacks the NH_2-terminal cysteine sites of palmitoylation. The differential effect of these β_{1a}- and β_2-subunits on voltage-dependent inactivation of the $\alpha_{1C,77}$ channel expressed in *Xenopus* oocytes has been described (Soldatov et al., 1997). These results confirmed other reports on the acceleration of the Ba^{2+} current decay by the β_{1a}-subunit as compared with β_2 (Birnbaumer et al., 1998; Colecraft et al., 2002). This β-subunit dependence of inactivation, defined here as differential β-subunit modulation of inactivation, may be associated with the different ability of β-subunits, permanently bound to AID, to freely move with the cytoplasmic linker between repeats I and II of the α_{1C}-subunit, thus serving as a voltage-dependent inactivation particle (Restituito et al., 2000).

The aim of this work was to investigate the correlation between the effects of β_{1a}- and β_2-subunits on inactivation of the $\alpha_{1C,77}$ and $\alpha_{1C,IS\text{-}IV}$ channels and the voltage-dependent rearrangements between the α_{1C}- and β-subunits using FRET microscopy combined with voltage clamp in live cells (Kobrinsky et al., 2003). This method of measuring the dynamic structural responses to changes in cell membrane potential was used to determine the differences in relative proximity and/or angular orientation between the NH_2-terminal regions of different α_{1C}- and β-subunits, as well as relative to the plasma membrane when channels are in the resting, inactivated, or conducting states.

MATERIALS AND METHODS

Molecular biology

Preparation of plasmids encoding $\alpha_{1C,77}$ (Soldatov et al., 1995) and $\alpha_{1C,IS\text{-}IV}$ (Shi and Soldatov, 2002) in pBluescript vector for expression in *Xenopus* oocytes and plasmids encoding $\alpha_{1C,77}$, β_{1a} (Mori et al., 1991), and $\alpha_2\delta$ (Singer et al., 1991) proteins in pcDNA3 vector for eukaryotic expression (Soldatov et al., 2000) has been described previously. All tagged α_{1C} channels retained characteristic electrophysiological properties of the untagged channels. The $(ECFP)_N$-β_{1a} expressing plasmid in a pcDNA3 vector (N stands for NH_2-terminus of a subunit) was prepared by a three-piece ligation. The 6.1-kb *Not* I/*Blp* I segment of pβ_1cDNA3 plasmid (Soldatov et al., 2000) was ligated with the ECFP-coding region containing the 5′-terminal *Not* I linker and the 3′-terminal *Xho* I linker attached by PCR, and 1-kb *Xho* I/*Blp* I fragment of the β_{1a}-coding plasmid pCaB1 (Mori et al., 1991) with the *Xho* I linker attached by PCR. The $(EYFP)_N$-β_{1a}-pcDNA3 expressing plasmid was obtained by replacing the *Not* I/*Xho* I ECFP-coding segment of $(ECFP)_N$-β_{1a}-pcDNA3 with the EYFP-coding region containing the 5′-terminal *Not* I linker and the 3′-terminal *Xho* I linker introduced by PCR. To prepare the $(ECFP)_N$-β_2 expressing plasmid, the *Avr* II/*Acc* I segment of the β_2-subunit coding region was ligated with the *Xba* I/*Acc* I-digested vector pUC18 (Life Technologies, Carlsbad, CA). The *Bam*H I/*Acc* I fragment of this construct was subcloned into *Bgl* II and *Acc* I sites of the pECFP-C1 vector (Clontech, Palo Alto, CA). Nucleotide sequences of all PCR products as well as ligation sites were confirmed at the DNA sequencing facility of the University of Maryland. Preparations of cRNA were obtained by in vitro transcription of the linearized vectors using T7/SP6 mMessage mMachine (Ambion, Austin, TX).

Cell cultures

COS1 cells used in experiments did not show appreciable endogenous expression of $Ca_v1.2$ channels (Meir et al., 2000). HEK293 cells were selected for immunoprecipitation and single-channel analyses (Kepplinger et al., 2000), because of the fast time course and high level of transient expression of recombinant $Ca_v1.2$ channels. COS1 cells are particularly useful for single-cell electrophysiology, because they divide slower than HEK293 cells and allow for tighter control over the efficiency of expression of proteins of different size. COS1 cells were grown on poly-D-lysine coated coverslips (MatTek, Ashland, MA) in DMEM supplemented with 10% fetal calf serum. HEK293 cells used for immunoprecipitation analysis and COS1 were transfected with cDNAs coding for the indicated α_{1C}-, β-, and $\alpha_2\delta$-subunits of the Ca^{2+} channel (1:1:1, w/w) using the Lipofectamine (Invitrogen, Carlsbad, CA) or Effectene kit (Qiagen, Venlo, The Netherlands), respectively. In some experiments with COS1 cells, $(ECFP)_N$- and $(EYFP)_N$-labeled PH domains (van der Wal et al., 2001) were coexpressed. HEK293 cells used for single-channel experiments were transfected 24–72 h before recordings with cDNAs coding for $\alpha_{1C,77}$ or $(EYFP)_N$–$\alpha_{1C,IS\text{-}IV}$–$(ECFP)_C$, β_{1a}-, β_2-, and $\alpha_2\delta$-subunits using SuperFect transfection reagent (Qiagen). Unlike the $\alpha_{1C,77}$ channel, inactivation of which was somewhat (≈15%) accelerated by the N-terminal EYFP labeling, the decay of the Ba^{2+} current through the $\alpha_{1C,IS\text{-}IV}$ was not significantly affected by the double ECFP/EYFP labeling (Kobrinsky et al., 2003). The rationale for using the cDNA coding for $(EYFP)_N$–$\alpha_{1C,IS\text{-}IV}$–$(ECFP)_C$ was to facilitate identification of the expressing cells. No functional expression of the $\alpha_{1C,77}$ or $\alpha_{1C,IS\text{-}IV}$ channels was observed in COS1 cells in the absence of β-subunits.

Immunoprecipitation analysis

HEK293 cells were transfected in 75-cm^2 flasks with the mixture of α_{1C}, $\alpha_2\delta$, and $(EYFP)_N$-labeled β_{1a} or $(ECFP)_N$-labeled β_2-subunits as described

above. After 48–72 h, the cells were collected in 0.5 ml of Tris-buffered saline (150 mM NaCl, 50 mM Tris-HCl, pH 8.0) containing a mixture of protease inhibitors composed of 1 mM PMSF, 1 mM DTT, and 5 μl of protease inhibitor cocktail (P8340, Sigma, St. Louis, MO). To remove ''orphan'' β-subunits, not associated with the membrane-bound α_{1C} channels, cells were quickly freeze-thawed three times and then permeabilized with digitonin (20 μg/ml) for 5 min at 4°C. Lyzed cells were pelleted for 30 min at 12,000 $\times$ g, 4°C and solubilized with 0.5% Nonidet P-40. The cell extract was centrifuged for 30 min at 12,000 $\times$ g, 4°C. Equal amounts of protein extracts, determined by BCA protein assay (Pierce, Rockford, IL), were diluted twofold with 0.3 M KCl containing 50 mM Tris-HCl, pH 8.0, the mixture of protease inhibitors, and 10% glycerol. Extracts were incubated overnight at 4°C on a rotary shaker with 10 μl of Living Color Full-Length A.V. polyclonal antibody (BD Biosciences Clontech) prebound to 60 μl of rProtein A Sepharose Fast Flow (Amersham Pharmacia Biotech AB, Uppsala, Sweden). Protein A-sepharose beads were washed at 4°C for 15 min with the wash buffer (0.2% Nonidet P40, 50 mM Tris-HCl, pH 8.0, and protease inhibitors) containing 0.5 M KCl, then quickly washed twice with 0.3 M KCl in wash buffer, and then 30 min with 0.15 M KCl in wash buffer. The resin was finally rinsed twice briefly with 0.5 M KCl in wash buffer, and the retained proteins were eluted by incubation for 5 min at 95°C with 40 μl of SDS-sample buffer containing 2% SDS, 10 mM Tris-HCl (pH 6.8), 7.5% sucrose, and 0.5 M 2-mercaptoethanol. Proteins were separated by SDS-gel electrophoresis on a precasted 4–12% gradient polyacrylamide gel (Invitrogen) and transferred to a 0.45-μm PVDF membrane (BioRad, Hercules, CA). The $(ECFP/EYFP)_N$-labeled β-subunits were identified on Western blots with Living Color monoclonal antibody JL-8 (1:4000 dilution, BD Biosciences Clontech), whereas the coprecipitated α_{1C}-subunits were detected with the affinity purified rabbit anti-α_{1C} calcium channel polyclonal antibody (1:10,000; Chemicon International, Temecula, CA) using an ECL Plus Western blotting detection system (Amersham Pharmacia Biotech). Expression of labeled β-subunits was routinely monitored by the conventional epifluorescent microscopy.

FRET imaging

Images were recorded in live transfected COS1 cells with a Hamamatsu digital camera C4742-95 (Hamamatsu City, Japan) mounted on the Nikon (Melville, NY) epifluorescent microscope TE200 (60 $\times$ 1.2 n.a. objective) equipped with multiple filter sets (Chroma Technology, Rockingham, VT). Excitation light was delivered by a 75-W Xenon lamp (Woburn, MA). C-Imaging (Compix, Tualatin, OR) and MetaMorph (Universal Imaging, Downingtown, PA) software were used to obtain and analyze FRET images. FRET was quantified with three filter sets: for EYFP cube, excitation filter 500/20 nm, dichroic beam splitter 515 nm, emission filter 535/30 nm; for FRET (ECFP/EYFP) cube, excitation 436/20 nm, dichroic beam splitter 455 nm, emission filter 540/30 nm; and for ECFP cube, excitation filer 436/20 nm, dichroic beam splitter 455 nm, emission filter 480/40 nm. Regions of interest (ROI) were selected from plasma membrane sites where there was obvious signal of fluorescence and little or no interference from fluorescence from the intracellular compartment. Selection of ROIs was carried out using the C-Imaging software where intensity (I) from three filter sets was determined after background subtraction. Fluorescence values were averaged across the ROI (with one ROI per cell). Inside the ROIs some areas did not show substantial FRET. These areas were also included in the analysis. The full scale of digitized resolution ranged from 0 to 255. Because fluorescence in ROIs, containing typically ~1000 pixels, was averaged, the signal/noise ratio was, respectively, increased by two to three orders and thus resolution of FRET detection was more refined. Corrected intensity of FRET (I_{FRET^c}) was calculated as $(I_{FRET} - I_{ECFP} \times 0.585 - I_{EYFP} \times 0.115)$, where bleed-through coefficients were experimentally determined by calibration according to Xia and Liu (2001). This calibration is based on the measurements of fluorescence of all ECFP- and EYFP-labeled constructs expressed in COS1 cells in all three filters set to determine bleed-through in CFP, YFP, and FRET filters (for additional details, see Kobrinsky et al., 2003). The typical values of corrected FRET varied from 10 to 40. To quantify FRET, we used a generally accepted correction method (Xia and Liu, 2001). Corrected FRET values were normalized against donor and acceptor levels: $N_{FRET} = (I_{FRET^c})/(I_{EYFP} \times I_{ECFP})^{1/2}$. Under these conditions, FRET was directly demonstrated with the positive control of the coexpressed mixture of EYFP- and ECFP-labeled pleckstrin homology (PH) domains of phospholipase Cδ1 (Kobrinsky et al., 2003). Acceptor photobleaching (on average >90% for 15 min with the 100-W mercury lamp) gave a FRET efficiency of 0.209 $\pm$ 0.054 (n = 17), calculated as $(I_{ECFP^*} - I_{ECFP}) / I_{ECFP^*}$, where I_{ECFP} and I_{ECFP^*} are the intensities of ECFP fluorescence before and after acceptor (EYFP) photobleaching. The relative changes in FRET signal were determined from the pairs of consecutive FRET acquisitions recorded at two different transmembrane voltages (−90 and +20 mV), stabilizing the channel in different functional states. Acquisitions of fluorescence were obtained during the application of a conditioning pulse with simultaneous recordings of the current at indicated voltages and within the time window, ranging from 50 to 300 ms. In a recent comprehensive study comparing different FRET measurement methods (Berney and Danuser, 2003), it has been shown that use of corrected FRET values to present relative changes in FRET signal is adequate if the ratio of donor (ECFP) to acceptor (EYFP) is $\geq$1. This requirement was fulfilled throughout our study. In some cases, the entire consecutive image was shifted by one or two pixels and required pixel-by-pixel adjustment using the first (reference) image with designated ROI. Such a shift could easily be detected by comparison with the borders of ROI designated for the reference image.

Acceptor (EYFP) photobleaching was performed with custom YFP photobleaching cube (Chroma Technology), consisting of a D535/50 $\times$ excitation filter and 100% mirror (instead of a dichroic one); this bleaching cube spared the CFP chromophore in control experiments. The 175-W Xenon lamp was used for illumination.

For illustration purposes, results of the ratio of FRET measurements, not limited just with ROI, are presented as fluorescence images. The first step in the processing of such an illustrating image is subtraction of the background, which is typically 10–12 units on the full fluorescence scale of 255 units. Background was measured in the part of the image that was not affected by cell fluorescence or in a separate dish containing nonfluorescent cells. EYFP and EYCFP images with subtracted background were fractionally subtracted from raw FRET images based on measurements of bleed-through coefficients. The fractional subtraction generated corrected FRET images, showing sensitized FRET in COS1 cells. Because C-Imaging software converted possible negative values of fluorescence to zero, after this procedure, an average ''corrected background'' was typically 0 or 1. Although subtraction of images recorded at −90 and +20 mV gives absolute changes of FRET, the ratio of images allows for comparison between different experiments and thus was used in our research. To obtain illustrating images of the FRET ratio at +20 mV/−90 mV, an empirical constant value, typically equal to 5 on the fluorescence scale, was added to each pixel of both images corrected by the background subtraction. This was required to avoid division by zero background fluorescence of a corrected image. With noise ranging from 0 to 12 and the full scale of the measurement at 255, this operation did not substantially affect the relationship between the processed image and the actual calculation of corrected FRET in ROI, which did not include such processing.

Electrophysiology

Three different types of electrophysiological measurements were used. Two-electrode voltage clamp recording of Ba^{2+} currents through the wild-type and mutated Ca^{2+} channels expressed in *Xenopus* oocytes was carried out as described previously (Shi and Soldatov, 2002). To inhibit Ba^{2+}-activated Cl^- current, the oocytes were injected with 50 nl of 100 mM 1,2-*bis*(*o*-aminophenoxy)ethane-N,N,N′,N′-tetraacetate (BAPTA)-Cs (pH 7.4) 30 min before recordings.

All FRET measurements were combined with whole-cell patch clamp. Patch-clamp recording of the Ba^{2+} current in COS1 cells was carried out using the Axopatch 200B amplifier (Axon Instruments, Union City, CA) 48–72 h after transfection. The extracellular bath solution contained (in mM): NaCl 100, $BaCl_2$ 20, $MgCl_2$ 1, glucose 10, HEPES 10, pH 7.4. The pipettes had resistance 3–6 MΩ and were filled with pipette solution containing (in mM): CsCl 110, MgATP 5, BAPTA 10, tetraethylammonium 20, cAMP 0.2, HEPES 20, pH 7.4 (Soldatov et al., 2000). Currents were sampled at 2.5–5 kHz and filtered at 1 kHz. Voltage protocols were generated and data were digitized, recorded, and analyzed using pClamp 8.1 software (Axon). Calculated parameters are means ± SEM. The unpaired *t*-test was used to compare the $\alpha_{1C,77}/\beta$ and $\alpha_{1C,IS\text{-}IV}/\beta$ channels.

In single-channel recordings, the bath solution contained (in mM): L-aspartic acid 110, KCl 20, $MgCl_2$ 2, EGTA 2, HEPES 20, pH 7.4 (KOH). The pipette solution contained (in mM): $BaCl_2$ 96, HEPES 5, pH = 7.4 (NaOH). The pipettes were made of borosilicate glass, coated with SigmaCote (Sigma) to reduce pipette capacitance, heat polished, and showed resistances of 3–4.5 MΩ. Voltage protocols were applied and single-channel current traces were recorded using pClamp 6 software (Axon). Interpulse potential was held at −80 mV for 5 s, after depolarization pulse to 0 mV (maximum of activity) for 1 s. Currents were sampled at 10 kHz and filtered at 1 kHz. Analysis of single-channel data (average open probability, N.p) was performed with Matlab software (MathWorks, Natick, MA) using algorithms according to Schmid et al. (1995) and Baumgartner et al. (1997). In experiments where more than one single channel was visible, the number of channels was estimated by the maximum number of overlapping openings seen within the 80–140 traces as described by Baumgartner et al. (1997). All measurements were carried out at 20–22°C.

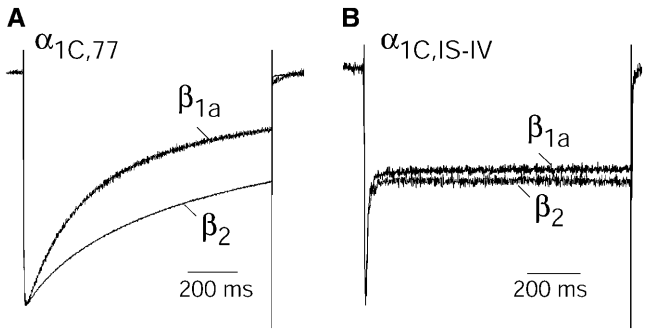

FIGURE 1 Differential β-subunit modulation of the voltage-dependent inactivation in the wild-type $\alpha_{1C,77}$ channel (*A*) and its lack in the $\alpha_{1C,IS\text{-}IV}$ channel (*B*). Shown are effects of coexpression of the β_{1a}- or β_2-subunits on inactivation of the Ba^{2+} currents recorded in *Xenopus* oocytes at the peak of current-voltage relationships (+10 mV) with holding potential of −90 mV and 40 mM Ba^{2+} in the perfusion solution. A two-exponential fitting of the Ba^{2+} current inactivation kinetics obtained from the analysis of the 1-s pulse traces showed that the fast time constant of the $\alpha_{1C,77}$ channel was not significantly changed ($p > 0.09$; unpaired *t*-test) when the β_{1a}-subunit ($\tau_f = 94.0 \pm 9.8$ ms, $n = 30$) was replaced by β_2 ($\tau_f = 132.0 \pm 18.6$ ms, $n = 17$). The slow time constant of the Ba^{2+} current inactivation kinetics was significantly ($p < 0.005$) increased when the β_{1a}-subunit ($\tau_s \approx 558 \pm 66$ ms) was replaced by the β_2-subunit ($\tau_s \approx 925 \pm 112$ ms) with the $\alpha_{1C,77}$ channel (*A*), but remained essentially unchanged in the case of the $\alpha_{1C,IS\text{-}IV}$ channel (*B*) (see text for details).

RESULTS

Lack of differential β-subunit modulation of the $\alpha_{1C,IS\text{-}IV}$ channel inactivation

For comparison with our previous results (Shi and Soldatov, 2002), the electrophysiological study of inactivation of the $\alpha_{1C,77}$ and $\alpha_{1C,IS\text{-}IV}$ channels were initially carried out in the *Xenopus* oocyte expression system. Expression in oocytes provided control over subunit composition of the Ca^{2+} channels and yielded results fully compatible with those acquired by the whole-cell patch clamp recording in COS1 cells used for the FRET microscopy (see below). Differential β-subunit modulation of the Ba^{2+} current through the wild-type ($\alpha_{1C,77}$) channel is illustrated in Fig. 1 *A* as a difference in kinetics of the current inactivation conveyed to the channel by coexpression of β_{1a}- and β_2-subunits. Replacement of the β_2-subunit with β_{1a} significantly accelerated decay of the Ba^{2+} current, which supports results of other studies reviewed by Birnbaumer et al. (1998).

Fig. 1 *B* shows results obtained with the $\alpha_{1C,IS\text{-}IV}$ channel coexpressed with the β_{1a}- and $\alpha_2\delta$-subunits in *Xenopus* oocytes. In complete agreement with our previous report (Shi and Soldatov, 2002), ≈50% of the maximum Ba^{2+} (or Ca^{2+}) current through the $\alpha_{1C,IS\text{-}IV}/\beta_{1a}$ channel was inactivated with a single-exponential decay ($\tau_f = 11.7 \pm 0.3$ ms; $n = 34$), did not show Ca^{2+}-dependent inactivation, and completely recovered from voltage-dependent inactivation within < 100 ms. The sustained fraction of the current (45.2 ± 2.1%, $n = 18$) lasted for up to 30 s without decay (Fig. 1*B*, *top trace*). Coexpression of the β_2-subunit instead of β_{1a} did not change the electrophysiological properties of the $\alpha_{1C,IS\text{-}IV}$ channel except for some increase (≈10%, $p < 0.05$) in the amplitude of the sustained Ba^{2+} current to 56.6 ± 4.4% ($n = 5$) of the peak current (Fig. 1 *B*, *bottom trace*). The time constant for the fast component of inactivation was not significantly changed ($\tau_f = 12.4 \pm 0.7$ ms; $n = 5$).

Data summarized in Fig. 2 show that none of the tested kinetics or voltage-dependent characteristics of the Ba^{2+} current through the $\alpha_{1C,IS\text{-}IV}$ channel were notably affected by the coexpression of the β_2-subunit instead of β_{1a}. The sustained current was observed over a wide range of membrane potentials (Fig. 2 *A*) and, on average, accounted for 50–55% of the peak current. No significant differences in the current-voltage relationships for the peak and sustained Ba^{2+} current or the time course of fast inactivation (Fig. 2 *B*) were found between the $\alpha_{1C,IS\text{-}IV}$ channels coexpressed with β_{1a}- and β_2-subunits. The values for half-maximal activation $V_{0.5} = 2.1 \pm 1.3$ mV (slope factor $k_{I\text{-}V} = -9.1 \pm 1.3$ mV; $n = 10$) with β_{1a} and 3.9 ± 2.0 ($k_{I\text{-}V} = -8.9 \pm 0.7$; $n = 3$) with β_2 were not significantly different ($p < 0.002$; unpaired *t*-test). The sustained Ba^{2+} current did not show decay even with prolonged depolarization (Fig. 2 *C*). Similar to the $\alpha_{1C,IS\text{-}IV}/\beta_{1a}$ channel, the $\alpha_{1C,IS\text{-}IV}/\beta_2$ channel was characterized by high steady-state availability at positive voltages (Fig. 2 *D*) and rapid recovery from inactivation within ≈100 ms (data not shown). Thus, it seems that inhibition of slow voltage-dependent inactivation interferes with differential β-subunit modulation of the kinetics of inactivation. Based on this observation, we hypothesize that

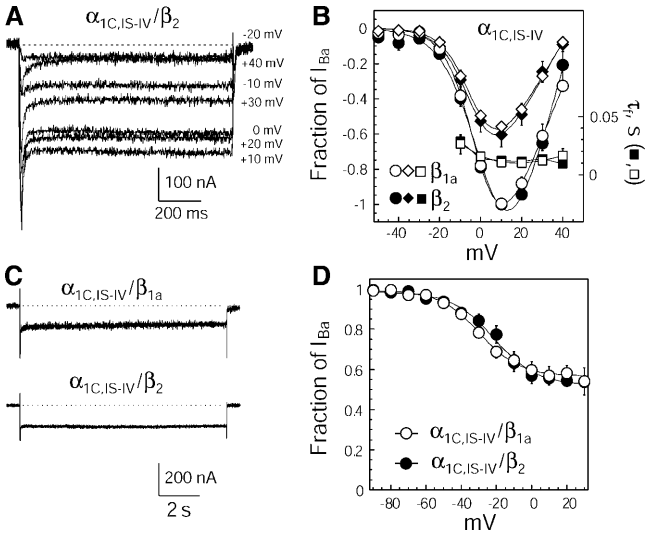

FIGURE 2 Electrophysiological properties of the mutated $Ca_v1.2$ channel composed of the $\alpha_{1C,IS-IV}$-, β_2-, and $\alpha_2\delta$-subunits coexpressed in *Xenopus* oocytes. (*A*) Traces of the Ba^{2+} current evoked by 1-s depolarizations in the range from −20 to +40 mV (10-mV increments) from a holding potential of −90 mV. (*B*) Comparison of the current-voltage relationships for the peak (*circles*) and sustained (*diamonds*) Ba^{2+} currents as well as the voltage dependence of the time constant of inactivation (τ_f, *squares*) for the $\alpha_{1C,IS-IV}/\beta_{1a}$ (*open symbols*, $n = 8$) and $\alpha_{1C,IS-IV}/\beta_2$ channels (*solid symbols*, $n = 3$) The curves were fitted by the equation $I_{Ba} = G_{max}\,(V - E_{rev})/\{1 + \exp[(V - V_{0.5})/k_{I-V}]\}$, where I_{Ba} is the amplitude of the Ba^{2+} current, G_{max}, the maximum conductance; E_{rev}, the reversal potential, $V_{0.5}$, the voltage at 50% of I_{Ba} inactivation, and k_{I-V}, the slope factor. (*C*) Lack of inactivation of the sustained current illustrated by a typical trace of the Ba^{2+} current through the $\alpha_{1C,IS-IV}/\beta_{1a}$ (*top*) and $\alpha_{1C,IS-IV}/\beta_2$ channels (*bottom*) induced by 10-s depolarization to +10 mV from a holding potential of −90 mV. (*D*) Comparison of steady-state inactivation curves for the peak Ba^{2+} current through the $\alpha_{1C,IS-IV}/\beta_{1a}$ (○, $n = 6$) and $\alpha_{1C,IS-IV}/\beta_2$ channels (●, $n = 3$). The curves were fitted by a Boltzmann function $I_{Ba} = a + b \times \{1 + \exp[(V - V_{0.5})/k]\}$, where V is the conditioning pulse voltage, $V_{0.5}$ is the voltage at half-maximum of inactivation, k is a slope factor, a and b are fractions of noninactivating and inactivating components of the Ba^{2+} current, respectively. $V_{0.5} = -27.7 \pm 1.5$ mV, $k = 14.7 \pm 3.0$, and $a = 52.1 \pm 4.6$ ($n = 7$) for the $\alpha_{1C,IS-IV}/\beta_{1a}$ channel. Respectively, for the $\alpha_{1C,IS-IV}/\beta_2$ channel, $V_{0.5} = -24.0 \pm 4.1$ mV, $k = 12.6 \pm 0.5$, and $a = 52.7 \pm 2.4$ ($n = 3$).

β-subunits modulate the kinetics of the Ba^{2+} current decay by targeting the slow inactivation mechanism of the channel.

Comparison of the effects of the β_{1a}- and β_2-subunits on $Ca_v1.2$ channels with different inactivation properties

To investigate whether the inhibition of slow inactivation of the $Ca_v1.2$ channel affects the interaction between the α_{1C}- and β-subunits, coimmunoprecipitation of the β_{1a}- or β_2-subunits with the wild-type $\alpha_{1C,77}$- and mutated $\alpha_{1C,IS-IV}$-subunits was analyzed by Western blot assay. The $(EYFP/ECFP)_N$-labeled β_{1a}- or β_2-subunits were functionally coexpressed in HEK293 cells with the $\alpha_2\delta$- and $\alpha_{1C,77}$- or $\alpha_{1C,IS-IV}$-subunits. Putative ''orphan'' cytosolic β-subunits not associated with membrane-bound α_{1C} were removed by cell lysis upon three cycles of freeze-thaw followed with brief permeabilization by low concentration of digitonin. The crude membrane particulate fraction of HEK293 cells contained ''orphan'' α_{1C}-subunits and those associated with the labeled β-subunits. The latter were immunoprecipitated from solubilized membranes as $\alpha_{1C}/(ECFP)_N$-β complexes by antibody against GFP variants, thus eliminating contamination with the ''orphan'' α_{1C}-subunits. The immunoprecipitated complexes of the $\alpha_{1C}/(ECFP)_N$-β-subunits were analyzed with SDS-polyacrylamide gel electrophoresis and immunoblotting (Fig. 3 *A*). Western blots showed that both types of the β-subunit pulled down the $\alpha_{1C,77}$ and $\alpha_{1C,IS-IV}$ proteins and thus confirmed physical association of the β_{1a}- or β_2-subunits with either channel. Supporting experiment with coimmunoprecipitation of the unlabeled β_{1a}- or β_2-subunits with the (EYFP)/(ECFP)-tagged $\alpha_{1C,77}$ and $\alpha_{1C,IS-IV}$ subunits corroborated this result (data not shown).

Recordings of the single-channel activity (Fig. 3 *B*) of $\alpha_{1C,77}$ and $\alpha_{1C,IS-IV}$ coexpressed with the $\alpha_2\delta$- and β_{1a}- or β_2-subunits in HEK293 cells provided insight into their gating behavior, particularly at the end of the 1-s depolarizing pulse where the differences in β-subunit modulation of inactivation become especially clear and where FRET images were taken (see below). It is evident (Fig. 3 *B*, *left*) that single-channel activity with the $\alpha_{1C,77}/\beta_2$ channel is sustained at the end of a 1-s depolarization in contrast to the rather low activity of the $\alpha_{1C,77}/\beta_{1a}$ channel. Confirming data obtained with macroscopic currents, the $\alpha_{1C,IS-IV}$ mutant with β_{1a} or β_2 showed a similar low activity that was independent of the type of the coexpressed β-subunit and was sustained during depolarization (Fig. 3 *B*, *right*). Consistent with this observation was the average open probability ($N.p$) of the Ba^{2+} current calculated for the time window of 800–950 ms at the end of each 1-s depolarization (Fig. 3 *C*). The $\alpha_{1C,77}/\beta_2$ channel demonstrated the highest $N.p_{800\text{-}950ms}$, whereas the $\alpha_{1C,77}/\beta_{1a}$ channel and $\alpha_{1C,IS-IV}$ coexpressed with either β_{1a}- or β_2-subunit show no significant difference in low $N.p_{800\text{-}950ms}$ values. These various patterns of activity ($N.p_{800\text{-}950ms}$) are not due to different number of channels N, but occurred rather due to different $p_{800\text{-}950ms}$, as evident from Fig. 3 *D*. Furthermore, the ratio of average open probabilities determined between the 0–50-ms and 800–950-ms time windows of each recording (Fig. 3 *B*, *boxed*) during a 1-s depolarization was significantly higher for the $\alpha_{1C,77}/\beta_{1a}$ channel compared to the other α_{1C}/β-subunit combinations (Fig. 3 *E*). This result corresponds to the most extensive inactivation of the $\alpha_{1C,77}/\beta_{1a}$ channel among the channels tested in the whole-cell experiments and is consistent with the similarly low extent of inactivation for the $\alpha_{1C,77}/\beta_2$ channel and those of $\alpha_{1C,IS-IV}$ coexpressed with either β_{1a}- or β_2-subunit. Taken together, these data indicate that mutation of ADSI does not abolish the stable association between β- and α_{1C}-subunits, but leads to the loss of differential β-subunit modulation of inactivation.

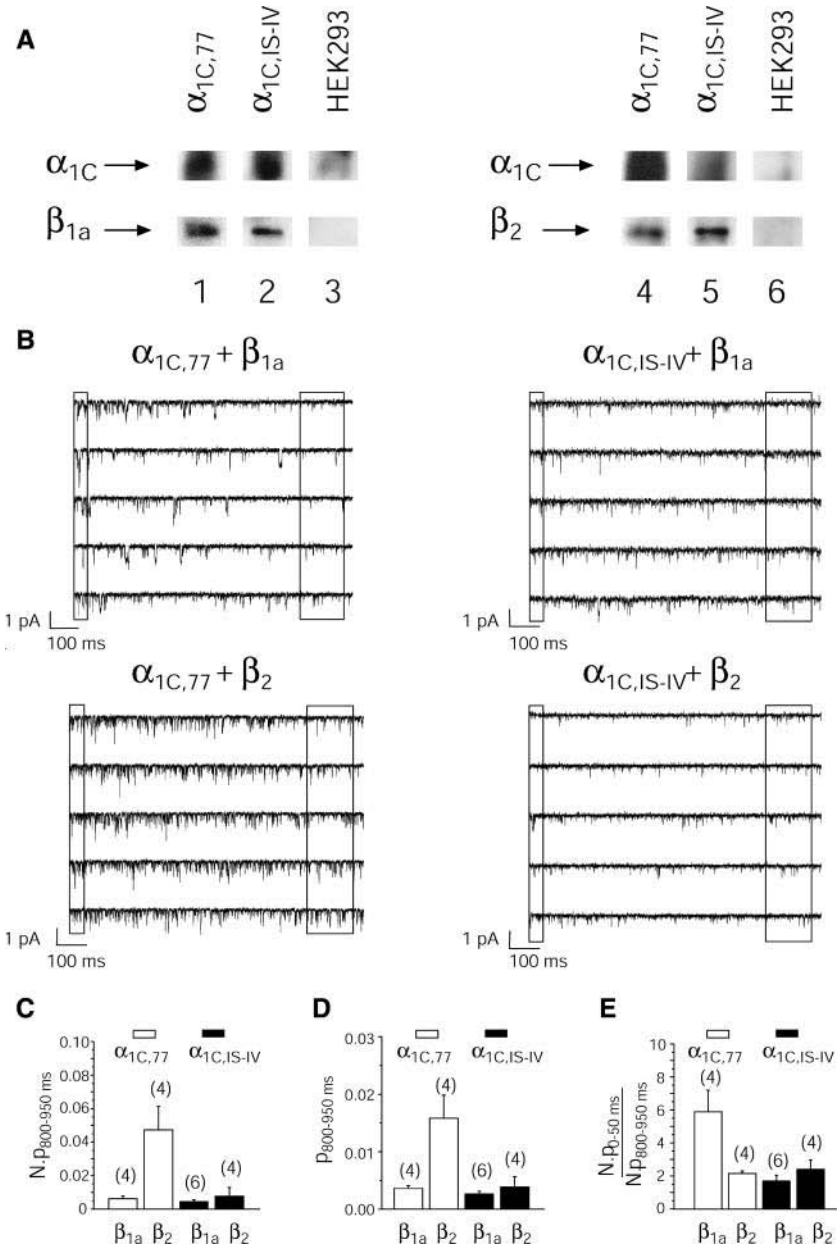

FIGURE 3 Effect of the β_{1a}- and β_2-subunits on the properties of the $\alpha_{1C,77}$ and $\alpha_{1C,IS\text{-}IV}$ channels. (*A*) Coimmunoprecipitation of the α_{1C}- and β-subunits in cells expressing the $\alpha_{1C,77}$ and $\alpha_{1C,IS\text{-}IV}$ channels. The (1,4) $\alpha_{1C,77}$- or (2,5) $\alpha_{1C,IS\text{-}IV}$- subunits, coexpressed with $\alpha_2\delta$ and (1,2) EYFP-labeled β_{1a}- or (4,5) ECFP-labeled β_2-subunits in HEK293 cells, were solubilized with Nonidet P-40, immunoprecipitated with polyclonal antibody to GFP in the presence of protein A-sepharose, and analyzed by Western blot for the β-subunits using monoclonal antibody to GFP, and for the α_{1C}-subunits by polyclonal anti-α_{1C} antibody (*arrows*). Controls (3,6) show nontransfected HEK293 cells. (*B*) Single-channel recordings of the $\alpha_{1C,77}$ or $(EYFP)_N$–$\alpha_{1C,IS\text{-}IV}$–$(ECFP)_C$ channel expressed with $\alpha_2\delta$- and β_{1a}- or β_2-subunits in HEK293 cells. Currents were elicited by 1-s depolarizations to 0 mV from the holding potential of −80 mV. Boxed are 0–50 ms and 800–950 ms episodes used for the subsequent analysis. Average open probabilities determined as $N.p$ (*C*) or p (*D*) at the 800–950 ms time window of a 1-s depolarization (boxed in *B*). For each independent experiment, between 80 and 140 traces were analyzed (number of experiments is shown in parentheses). Only the average open probability for $\alpha_{1C,77}/\beta_2$ channel was significantly ($p < 0.05$) different to the other α_{1C}/β channels. (*E*) Ratio of average open probabilities (determined as $N.p$) between the 0–50-ms and 800–950-ms time windows (*boxed* in *B*) during a 1-s depolarization. Only the ratio calculated for the $\alpha_{1C,77}/\beta_{1a}$ channel was significantly ($p < 0.05$) different from the other α_{1C}/β channels.

Voltage-dependent rearrangement between the $\alpha_{1C,77}$- and β_{1a}-subunits

FRET is a result of the molecular interaction between the labeled partners (Lakowicz, 1999). FRET measurement with simultaneous voltage clamp gives an opportunity to eliminate possible artifacts associated with ''orphan'' subunits in live cells and focus exclusively on tagged α_{1C}- and β-subunits of fully functional channels. One of the most commonly used approaches is to measure FRET efficiency by acceptor photobleaching. Specially designed Chroma D535/50 × excitation filter (Erickson et al., 2003) provided ≈90% photobleaching of EYFP in 2 min, a time sufficient to determine FRET efficiency under conditions when stability of a patch is not compromised. Recently Tour et al. (2003) reported on the high photosensitivity of labeled $Ca_v1.2$ channel to rundown. We found that EYFP photobleaching greatly accelerated rundown of the $(EYFP)_N$-$\alpha_{1C,77}$ channel activity (data not shown) and thus can't be applied to the measurements of voltage-gated changes of FRET, because of uncertainty in the functional state of the channel.

To overcome this problem, we used another widely accepted approach based on FRET determination by correction methods, and combined patch clamp with FRET microscopy. The directly measured FRET intensity was corrected for the cross talk from the donor and the acceptor and by the background. FRET ratio was determined independently from donor and acceptor concentrations and

additionally normalized to the direct donor and acceptor intensity according to Xia and Liu (2001). Fluorescence images *b* and *c* (Fig. 4 *A*) indicate that coexpressed $(ECFP)_N$-β_{1a} and $(EYFP)_N$-$\alpha_{1C,77}$ subunits are similarly distributed in the cell. We focused our analysis on the plasma membrane region, where the voltage-gated functional channel molecules reside. A FRET measurement of the same cell recorded at −90 mV (*panel d*) shows that N_{FRET} between these subunits was rather small. Depolarization to +20 mV (Fig. 4 *A*, *panel e*) resulted in a substantial increase in N_{FRET} between the $(ECFP)_N$-β_{1a} and $(EYFP)_N$-$\alpha_{1C,77}$ subunits (Table 1), which was confined to the rim of the cell, consistent with plasma membrane localization (see digitally magnified regions at the bottom of the whole-cell images).

FRET experiments were designed to estimate energy transfer between the fluorophores of the interacting subunits that was exclusively the result of structural rearrangements of the channel induced by the controlled changes of transmembrane voltage. When a cell is maintained at the holding potential of −90 mV, the $(ECFP)_N$-β_{1a}/$(EYFP)_N$-$\alpha_{1C,77}$ channels are in the resting closed state characterized by low FRET (Table 1). Depolarization to +20 mV, corresponding to the maximum of the current-voltage relationship, induced opening of the $(ECFP)_N$-β_{1a}/$(EYFP)_N$-$\alpha_{1C,77}$ channels followed by their voltage-dependent inactivation recorded as a rapid decay of the Ba^{2+} current. Therefore, the +20 mV image (Fig. 4 *A*, *panel e*) corresponding mainly to the inactivated state of the channels was recorded only after inactivation was essentially complete (i.e., the whole-cell current decayed to the dotted line, which marks the initial zero level of the current). The respective time window for the acquisition of the +20 mV image is labeled by the red bar above the current trace on Fig. 4 *A*. The ratio of the two consecutive images recorded at –90 and +20 mV (Fig. 4 *A*, *panel f*) represents only those changes in FRET that were due to the voltage-gated rearrangements in the channel from the resting to the predominantly inactivated state. Measured FRET correlates with the state of the channel, because reversible changes of FRET between $(EYFP)_N$-$\alpha_{1C,77}$ and $(ECFP)_N$-β_{1a} were observed every time inactivation had developed in response to depolarization from −90 mV to +20 mV.

When coexpressed with the unlabeled $\alpha_{1C,77}$- and $\alpha_2\delta$-subunits, the $(ECFP)_N$-labeled β_{1a}- and β_2-subunits did not show voltage-dependent changes in ECFP fluorescence. The ratio of ECFP fluorescence intensity measured at +20 mV to those at −90 mV did not significantly differ from 1.0 and was found to be 0.991 ± 0.006 ($n = 44$) with $(ECFP)_N$-β_{1a}/$\alpha_{1C,77}$; 1.018 ± 0.016 ($n = 40$) with $(ECFP)_N$-β_2/$\alpha_{1C,77}$; 1.006 ± 0.004 ($n = 22$) with $(ECFP)_N$-β_{1a}/$\alpha_{1C,IS\text{-}IV}$, and 0.997 ± 0.008 ($n = 22$) with $(ECFP)_N$-β_2/$\alpha_{1C,IS\text{-}IV}$. Conversely, acceptor (EYFP) fluorescence measured at +20 mV was not significantly different from those at −90 mV when the $(EYFP)_N$-labeled $\alpha_{1C,77}$- and $\alpha_{1C,IS\text{-}IV}$-subunits were coexpressed with the unlabeled β_{1a}- and β_2-subunits. Because a voltage-induced change of the acceptor fluorescence in EYFP cube will be subtracted from the FRET cube measurement, we did not expect a decline of the EYFP fluorescence ratio at +20 and −90 mV from 1 with our three-cube filter system even if acceptor hypothetically shows voltage-sensitive change of fluorescence. Indeed, the ratio of EYFP fluorescence intensity measured at +20 mV to those at −90 mV was on average not different from 1.0: 1.003 ± 0.007 ($n = 38$) with $(EYFP)_N$-$\alpha_{1C,77}$/β_{1a}; 1.002 ± 0.007 ($n = 10$) with $(EYFP)_N$-$\alpha_{1C,IS\text{-}IV}$/β_{1a}; 0.995 ± 0.010 ($n = 26$) with $(EYFP)_N$-$\alpha_{1C,77}$/β_2, and 1.011 ± 0.011 ($n = 16$) with $(EYFP)_N$-$\alpha_{1C,IS\text{-}IV}$/β_2. This control indicates that voltage-dependent changes of fluorescence of the individual ECFP or EYFP fluorophores fused to the NH_2-termini of the α_{1C}- and β-subunits do not contribute to the voltage-dependent changes in FRET between them recorded in this study.

Efficiency of FRET depends on the distance between the donor and acceptor fluorophores and their mutual angular orientation. Although $(ECFP)_N$-β and $(EYFP)_N$-α_{1C} subunits were expressed at 1:1 molar ratio, the uncertainties in their relative concentration can be minimized by the ratiometric analysis of FRET (Xia and Liu, 2001). Relative changes in normalized FRET values (N_{FRET}) were detected for all combinations of the α_{1C}- and β-subunits, with the exception of the $\alpha_{1C,77}$/β_2 channel (Table 1; Figs. 4, *B* and *C*). In the resting state (−90 mV), all tested channels were characterized by low FRET between the tagged NH_2-termini of the α_{1C}- and β-subunits. Depolarization to +20 mV caused almost complete inactivation of the $(EYFP)_N$-$\alpha_{1C,77}$/$(ECFP)_N$-β_{1a} channels within ≈1 s (see *current trace* in Fig. 4 *A*) and produced a fully reversible significant increase in N_{FRET} (Table 1; Fig. 4 *A*, *panel e*) measured in the predominantly inactivated state (marked by *red bar* above the current trace). This result suggests substantial rearrangement between the α_{1C}- and β-subunits in the inactivated state accompanied by a reduction of the apparent distance between the donor and acceptor fluorophores and/or more parallel orientation of the respective dipoles.

Voltage-dependent rearrangements between the $\alpha_{1C,77}$- and β_2-subunits

Replacement of the β_{1a}-subunit for β_2 produced an increase in the Ba^{2+} current amplitude corresponding to higher efficiency of expression of the $\alpha_{1C,77}$ channel. Complete inactivation of the Ba^{2+} current through the $\alpha_{1C,77}$/β_2 channel was delayed, even with a 45-s depolarization at +20 mV (Fig. 4*B*, *bottom trace* in the *left* panel), but not inhibited like in the case of the $\alpha_{1C,IS\text{-}IV}$ channel. No measurable current was observed when $\alpha_{1C,77}$ was expressed in COS1 cells in the absence of β-subunits (data not shown), thus precluding comparison of the current decay in the absence of the β-subunit modulation. Fluorescence measurements

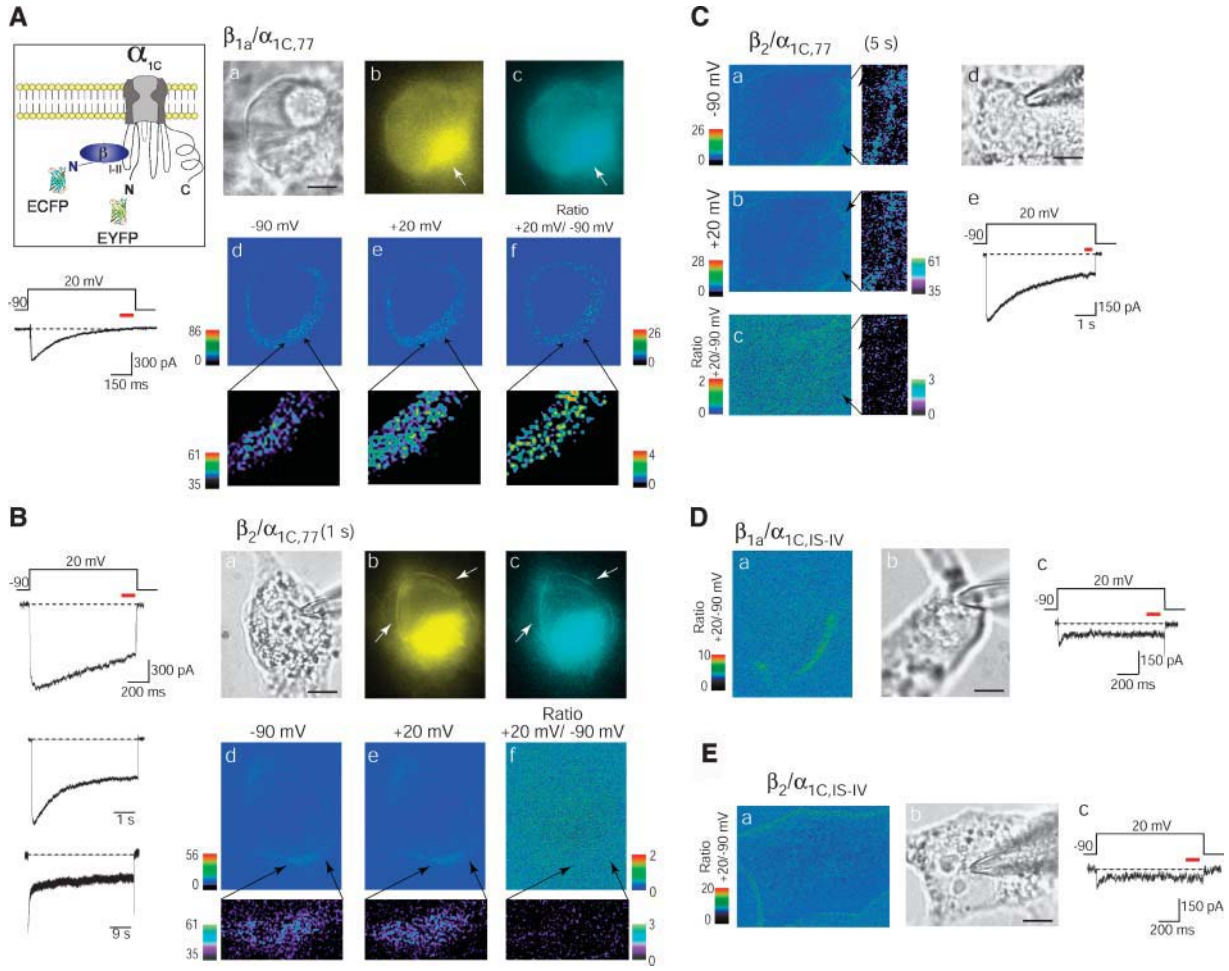

FIGURE 4 Voltage-gated rearrangements between the $(ECFP)_N$-β and $(EYFP)_N$-α_{1C} subunits of the functional Ca^{2+} channels determined by FRET combined with patch clamp in COS1 cells. (*A* and *B*) Voltage-dependent corrected FRET between the $(EYFP)_N$-$\alpha_{1C,77}$ and (*A*) $(ECFP)_N$-β_{1a} or (*B*) $(ECFP)_N$-β_2 subunits. Schematic diagram (*boxed*) depicts the arrangement of fluorophores. Panel *a*, phase-contrast cell image with a shadow of patch pipette. Panels *b* and *c*, images of the same cell with YFP and CFP filters, respectively. Arrows point to the plasma membrane distribution of the labeled proteins. Panels *d* and *e*, representative corrected images of FRET between the $(ECFP)_N$-β and $(EYFP)_N$-$\alpha_{1C,77}$ subunits recorded, respectively, at the resting (−90 mV) and inactivated ($(ECFP)_N$-β_{1a}) or predominantly conducting ($(ECFP)_N$-β_2) states of the channel (+20 mV). The time window of the +20-mV acquisition is marked on the left panel above the 1-s Ba^{2+} current trace by a red horizontal bar. Panel *f*, ratio of images *e*/*d* showing the voltage-dependent change of corrected FRET. Image areas indicated by arrows were digitally magnified to demonstrate the confinement of FRET to the plasma membrane. Three traces of the Ba^{2+} current on the left panel in *B*, recorded in response to the 1-, 5- and 45-s depolarizations, demonstrate that inactivation was not complete, and FRET imaging on panel *c* represents channels almost equally distributed between the inactivated and open states (ratio of the Ba^{2+} current after 1 s to the peak current, $r_{1s} \approx 0.56$). (*C*) Absence of marked FRET between the $(ECFP)_N$-β_{2a} and $(EYFP)_N$-$\alpha_{1C,77}$ subunits at the end of a 5-s depolarization to +20 mV that caused an additional decrease in the fraction of open channels ($r_{5s} \approx 0.33$). Panels *a* and *b*, representative corrected images of FRET obtained at −90 mV and +20 mV at the end of a 5-s pulse at the time window marked by the red bar above the current trace (*panel e*). Panel *c*, the ratio of corrected FRET images *b*/*a* sequentially recorded at +20 and −90 mV; right panels, digitally magnified areas of the image pointed by arrows. Panel *d*, phase-contrast image of the expressing cell with a shadow of patch pipette. (*D* and *E*) Voltage-dependent corrected FRET between the $(EYFP)_N$-$\alpha_{1C,IS-IV}$ and $(ECFP)_N$-β_{1a} (*D*) or $(ECFP)_N$-β_2 (*E*) subunits shown as a ratio of the sequentially recorded +20 mV/−90 mV images (panel *a*). Panel *b*, phase-contrast images of the expressing cell. Note that in every case the Ba^{2+} current recordings (shown below the respective images) provide evidence that the sustained conducting state was achieved before the +20-mV FRET image acquisitions (at time windows marked by *red bars*). Scaling bars, 5 μm.

corroborate the results of the immunoprecipitation/Western blot analysis and additionally confirm the expression of the β_2-subunit and its association with $\alpha_{1C,77}$. In the case of the $(EYFP)_N$-$\alpha_{1C,77}$/$(ECFP)_N$-β_2 channel, equally strong ECFP and EYFP fluorescence was observed (Fig. 4 *B*, *panels b* and *c*), similar to that found for the $(EYFP)_N$-$\alpha_{1C,77}$/$(ECFP)_N$-β_{1a} channel (compare with Fig. 4 *A*, *panels b* and *c*). Moreover, FRET images (Fig. 4 *B*, *panels d* and *e*, and the respective digitally magnified membrane regions) clearly point to colocalization of the labeled $\alpha_{1C,77}$- and β_2-subunits (notice different scale in FRET images when comparing Fig. 4 *B* with Fig. 4 *A*, *panels d–f*). Taken together, the large amplitude of the Ba^{2+} current, the immunoprecipitation analysis, the equally strong expression of the fluorescent $\alpha_{1C,77}$- and β_2-subunits, and their colocalization by FRET suggest that the low state-dependent change in FRET de-

TABLE 1 Voltage-dependent changes of normalized FRET between the $(ECFP)_N$-β and $(EYFP)_N$-α_{1C} subunits determined at −90 mV and +20 mV under whole-cell voltage clamp in COS1 cells

Ca channel subunits	$\beta_{1a}/\alpha_{1C,77}$	$\beta_2/\alpha_{1C,77}$	$\beta_{1a}/\alpha_{1C,IS\text{-}IV}$	$\beta_2/\alpha_{1C,IS\text{-}IV}$
−90 mV	0.01 ± 0.01	0.01 ± 0.005	0.02 ± 0.01	−0.02 ± 0.03
+20 mV	0.09 ± 0.02	−0.01 ± 0.01	0.17 ± 0.04	0.19 ± 0.03
Paired *t*-test	$p < 0.05$ ($n = 4$)	*ns* ($n = 39$)	$p < 0.05$ ($n = 6$)	$p < 0.01$ ($n = 10$)

Averages were compiled from different cells, where *n* stands for the number of cells. *p*, paired *t*-test; *ns*, nonsignificant difference.

termined for the ratio of images recorded at +20/−90 mV (Fig. 4 *B*, *panel f*) was not due to the lack of functional expression of the $(EYFP)_N$-$\alpha_{1C,77}$/$(ECFP)_N$-β_2 channel.

Insignificant change in relative N_{FRET} (Table 1) recorded at the end of the 1-s depolarization pulse to +20 mV from the holding potential of −90 mV (marked by the *red bar* above the *top current trace* in Fig. 4 *B*) corresponded to a transition of the $(EYFP)_N$-$\alpha_{1C,77}$/$(ECFP)_N$-β_2 channel from the resting to a predominantly noninactivated state, as seen from the slow and incomplete decay of the whole-cell Ba^{2+} current and single-channel-gating behavior in Fig. 3, *B* and *C*. An average fraction of inactivated channels in the 1-s recordings accounted for ≈44%. Prolongation of +20 mV depolarization pulse to 5 s (Fig. 4 *C*) increased the fraction of the inactivated channels to ≈67%. In the case of the $(EYFP)_N$-$\alpha_{1C,77}$/$(ECFP)_N$-β_{1a} channel, a similar fractional inactivation would correspond to almost fivefold increase in relative N_{FRET}. However, differential FRET between the $(EYFP)_N$-$\alpha_{1C,77}$ and $(ECFP)_N$-β_2 subunits recorded at −90 mV before and at the end of the 5-s pulse to +20 mV (Fig. 4 *C*, *panel c*) was not substantially increased. Thus, in sharp contrast with the β_{1a}-subunit, no significant voltage-dependent changes of FRET between the NH_2-terminal fluorescent tags of the $\alpha_{1C,77}$- and β_2-subunits were found. This result suggests that the voltage-gated rearrangements of the labeled parts in the $(EYFP)_N$-$\alpha_{1C,77}$/$(ECFP)_N$-β_2 channel complex are either insignificantly small or occur outside the detection limits of the method (i.e., when linear distance between the fluorophores becomes >10 nm, or the dipoles approach perpendicular orientation, or both). Overall, the difference in voltage-dependent FRET between $(EYFP)_N$-$\alpha_{1C,77}$ and the $(ECFP)_N$-labeled β_{1a}- or β_2-subunits (Table 1) reflects the differential β-subunit modulation of inactivation of the $\alpha_{1C,77}$ (''wild-type'') calcium channel.

Voltage-dependent rearrangement between $\alpha_{1C,IS\text{-}IV}$ and different β-subunits

In full agreement with the data obtained in oocyte expression system, the replacement of the β_{1a}-subunit for β_2 did not affect the kinetics of inactivation of the Ba^{2+} current through the $\alpha_{1C,IS\text{-}IV}$ channel expressed in COS1 cells (compare *current traces* in *panels c* in Fig. 4, *D* and *E*). On average, the fast time constant of inactivation was 13.0 ± 1.2 ms ($n = 13$) with the β_{1a}-subunit and 12.9 ± 0.8 ms ($n = 12$) with the β_2-subunit. The sustained fraction of the current (52 ± 8% with β_{1a} and 50 ± 9% with β_2) lasted for the duration of depolarization (up to 30 s) without decay. The relatively small current amplitudes obtained with the $\alpha_{1C,IS\text{-}IV}$ channel is characteristic for other $Ca_v1.2$ channel mutants with impaired Ca^{2+}-induced inactivation property (Soldatov et al., 1998). This was found to be due to a lower open probability and 10–15% reduction in the single-channel conductance (Kepplinger et al., 2000), and had no significant impact on the measurement of intramolecular FRET between the termini of the $\alpha_{1C,IS\text{-}IV}$ channel (Kobrinsky et al., 2003).

The lack of differential β-subunit modulation of the $\alpha_{1C,IS\text{-}IV}$ channel inactivation correlated with the absence of the β-subunit specificity of voltage-dependent FRET between the $(ECFP)_N$-β and $(EYFP)_N$-$\alpha_{1C,IS\text{-}IV}$ subunits. N_{FRET} between the NH_2-terminal tags of the $\alpha_{1C,IS\text{-}IV}$- and either β-subunits was found to increase in the sustained conducting state (Fig. 4, *D* and *E*; Table 1). However, this increase in FRET essentially did not depend on the type of the coexpressed β-subunit. The transition of the $(EYFP)_N$-$\alpha_{1C,IS\text{-}IV}$ channel into the conducting noninactivated state, stabilized by depolarization to +20 mV (Fig. 4, *D* and *E*, *panels c*), showed an equally large (by unpaired *t*-test) increase in N_{FRET} with either $(EYFP)_N$-β_{1a} (to 0.17 ± 0.04) or $(EYFP)_N$-β_2 subunit (to 0.19 ± 0.03). This result may reflect the loss of the β-subunit specificity of voltage-dependent rearrangements between the NH_2-terminal regions of the $\alpha_{1C,IS\text{-}IV}$- and β-subunits and correlates with the lack of differential β-subunit modulation of the Ba^{2+} current through the $\alpha_{1C,IS\text{-}IV}$ channel.

Voltage-dependent rearrangements of the α_{1C}- and β-subunits vis-à-vis the plasma membrane

FRET microscopy combined with whole-cell patch clamp was used to estimate whether the relative proximity of the α_{1C}- and β-subunits to the plasma membrane is changed in different functional states of the channel (Fig. 5). As membrane probes we used the ECFP/EYFP-labeled pleckstrin homology (PH) domains of phospholipase Cδ1 (van der Wal et al., 2001) that localize via PIP_2 to the inner leaflet of the plasma membrane. Unlike the $\alpha_{1C,77}$-$(ECFP)_C$ channel labeled at the C-terminal tail (Kobrinsky et al., 2003), which did not show FRET with the labeled PH domains (data not shown), all NH_2-terminally labeled α_{1C}- and β-subunits showed substantial FRET (Fig. 5 *A*). This finding suggests

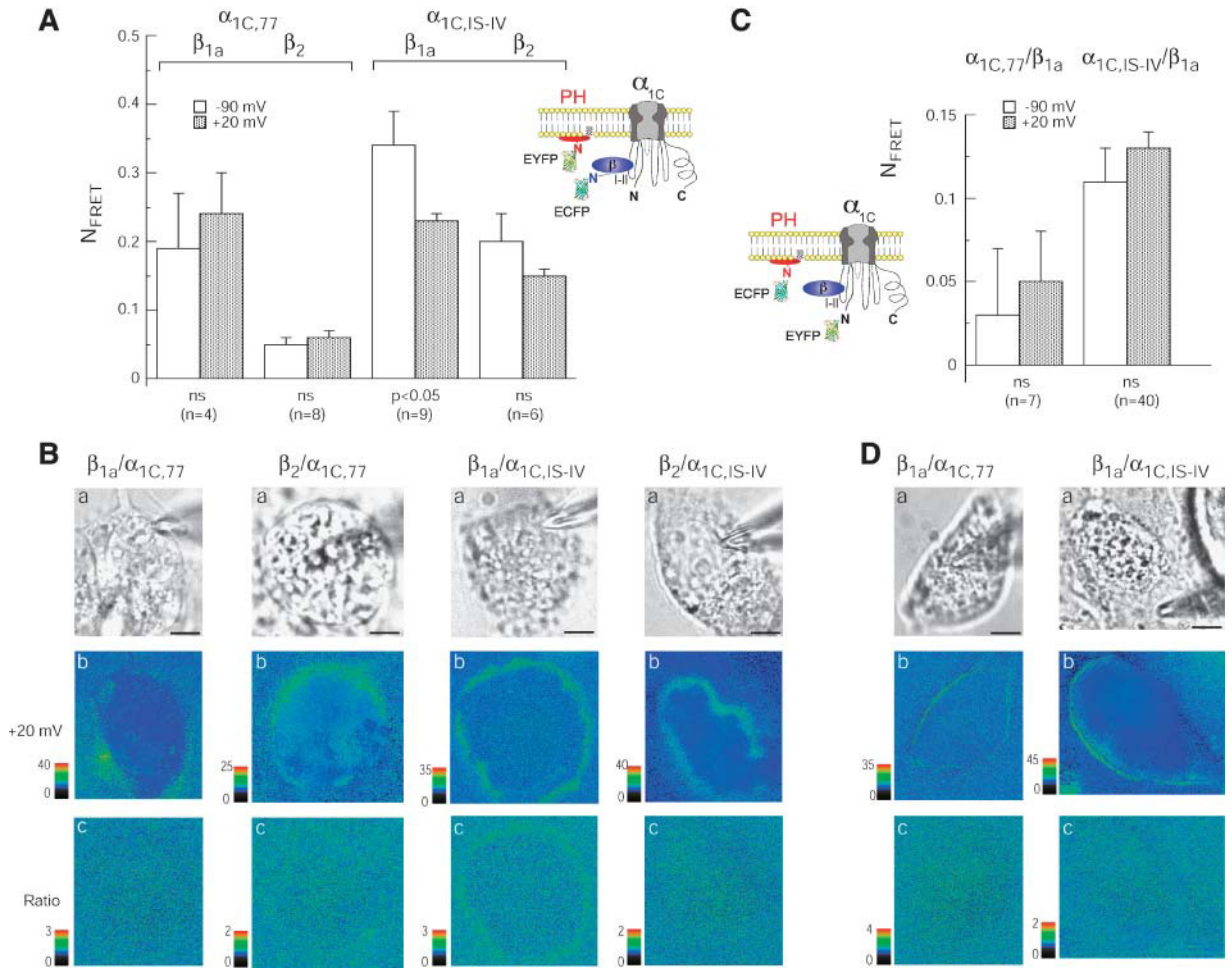

FIGURE 5 Voltage-dependent mobility of the NH_2-labeled α_{1C}- and β-subunits vis-à-vis the plasma membrane. (*A*) Comparison of normalized FRET between $(EYFP)_N$-PH and the indicated $(ECFP)_N$-β subunits in the $\alpha_{1C,77}$ or $\alpha_{1C,IS-IV}$ channels at −90 mV (*open bars*) and +20 mV (*shaded bars*) (conditions of FRET acquisition were similar to those in Figure 4). n, number of cells; p, paired *t*-test; ns, nonsignificant differences. Schematic diagram (inset) depicts the arrangement of fluorophores. (*B*) Representative FRET microscopy data corresponding to the paired bars in panel *A*. Panels *a*, phase-contrast images of the expressing cells, panels *b*, images of corrected FRET recorded at +20 mV, and panels *c*, ratio of FRET images sequentially recorded at +20 and −90 mV. (*C*) Comparison of normalized FRET between the indicated $(EYFP)_N$-α_{1C} subunits and $(ECFP)_N$-PH recorded at steady state at −90 mV (*open bars*) and +20 mV (*shaded bars*). Inset diagram shows the arrangement of fluorophores. (*D*) Panels *a*, phase-contrast images of the expressing cells. Panels *b* and *c* show the corresponding representative corrected FRET at +20 mV and the ratio of FRET images sequentially recorded at +20 and −90 mV, respectively. Scaling bars, 5 μm.

that the NH_2-termini of the α_{1C}- and β-subunits are situated near the plasma membrane within the linear detection limits of the method (≤100 Å), i.e., close enough to determine their state-dependent rearrangements with regards to the lipid bilayer.

The results of the measurements of the voltage-dependent rearrangements of β-subunits vis-à-vis the plasma membrane are shown in Fig. 5, *A* and *B*. FRET was measured between the donor fluorophore of $(ECFP)_N$-β and the acceptor fluorophore of $(EYFP)_N$-PH. The latter was expressed at ≈1:1 molar ratio to an $(ECFP)_N$-β subunit, and distributed predominantly over the cytoplasmic surface of the plasma membrane, most likely in a random and homogeneous manner. Control experiments showed that there was no FRET between $(EYFP)_N$-PH and $(ECFP)_N$-β unless the latter was coexpressed with the untagged α_{1C}- and $\alpha_2\delta$-subunits as a part of the channel complex. In the absence of membrane-anchoring α_{1C}-and $\alpha_2\delta$-subunits, the labeled β_{1a}- and β_2-subunits exhibited similarly diffuse distribution in the cytoplasm without preferential targeting of the plasma membrane (data not shown). However, as parts of the functional Ca^{2+} channel, $(ECFP)_N$-labeled β-subunits displayed strong FRET with $(EYFP)_N$-PH domain (Fig. 5 *A*). This FRET was probably due to not only the close proximity and the effective alignment of the fluorophores, but also the global or local deviation from the 1:1 donor/acceptor ratio (Lakowicz, 1999; Xia and Liu, 2001). Therefore it would be incorrect to compare individual FRET measurements obtained at a single potential, e.g., +20 mV (Fig. 5 *B*, *panels b*). To compensate for possible artifacts, ratios were

calculated from FRET images that were sequentially recorded at −90 and +20 mV (Fig. 5 *B*, *panel c*). Using this approach, it was found that none of the β-subunits showed a state-dependent change of FRET, with the possible exception of $(ECFP)_N$-β_{1a} in the $\alpha_{1C,IS-IV}$ channel (Fig. 5 *A*). Assuming randomized orientation of the independent fluorophores (see *scheme* in Fig. 5 *A*), one may conclude that the NH_2-termini of either the β_{1a}- or β_2-subunit of the functional $\alpha_{1C,77}$ channel do not significantly change their proximity with respect to the plasma membrane in response to depolarization. Inhibition of slow inactivation in the $\alpha_{1C,IS-IV}$ channel may facilitate the voltage-gated mobility of the $(ECFP)_N$-β_{1a} subunit, which is not associated with inactivation of the channel.

Fig. 5, *C* and *D*, show that FRET between the $(ECFP)_N$-PH domain and the $(EYFP)_N$-tagged $\alpha_{1C,77}$ or $\alpha_{1C,IS-IV}$ channels containing the β_{1a}-subunit is essentially voltage independent. No significant changes in FRET between the NH_2-terminal fluorophores of the α_{1C}-subunits and the plasma membrane PH domain probes were observed for the channels in the resting and the inactivated ($\alpha_{1C,77}$) or conducting ($\alpha_{1C,IS-IV}$) states.

DISCUSSION

Results of our work show that voltage-gated rearrangements between the NH_2-termini of the α_{1C}- and β-subunits, associated with inactivation of the $Ca_v1.2$ channel, depend on ADSI, the type of the β-subunit, and differential β-subunit modulation of inactivation.

Differential β-subunit modulation and slow inactivation

The effect of β-subunits on the kinetics of the Ba^{2+} current decay is mediated by their interactions with the ion-conducting α_{1C}-subunits. However, is not clear whether inactivation of the $Ca_v1.2$ channel is inherent to association between the α_{1C}- and β-subunits. Earlier, Ferreira et al. (1997) observed in tsA201 cells an expression of the functional cardiac rabbit α_{1C} channel in the absence of the rat brain β_2-subunit. In their report, a coexpression of the β_2-subunit predominantly affected the amplitude of the Ba^{2+} current but did not accelerate the kinetics of inactivation. In contrast, our studies in COS1 cells showed no functional expression of the $\alpha_{1C,77}$ and $\alpha_{1C,IS-IV}$ channels in the absence of β-subunits. Thus, we investigated the β-subunit modulation of inactivation as a differential effect of two different β-subunits, β_{1a} and β_2, on two variants of the $Ca_v1.2$ channels showing completely different inactivation properties.

Inactivation of the Ba^{2+} current through the ''wild-type'' $\alpha_{1C,77}$ channel is characterized by fast and slow components and is subject to differential β-subunit modulation (Fig. 1 *A*). Inhibition of the voltage-dependent slow inactivation ($\alpha_{1C,IS-IV}$) abolished differential β-subunit modulation of the Ba^{2+} current (Fig. 1 *B*). The replacement of the β_{1a}-subunit with β_2 did not cause appreciable changes in the inactivation kinetics of the $\alpha_{1C,IS-IV}$ channel over a wide range of membrane potentials (Figs. 2 and 3 *B*) and produced only marginal reduction of the fast component of the current (Fig. 1 *B*). This result is not due to a disruption of physical association between the α_{1C}- and β-subunits. The immunoprecipitation assay (Fig. 3 *A*) and direct measurements of FRET between the β- and α_{1C}-subunits (Fig. 4, *A* and *B*, *panels d* and *e*) independently confirmed their colocalization. Given the strong structural binding of β-subunits to the AID locus of the I-II linker of the α_{1C}-subunit (Pragnell et al., 1994; De Waard et al., 1994), this result is not surprising, because the I-II linker remains unchanged in the tested α_{1C}-subunits. Taken together, these findings suggest that association of β-subunits with AID is not sufficient for differential β-subunit modulation of inactivation that seems to selectively target the slow inactivation of the $\alpha_{1C,77}$ channel, a mechanism that is inhibited in the $\alpha_{1C,IS-IV}$ channel.

Structural rearrangements between the α_{1C}- and β-subunits

The second essential finding of this study shows that the differential β-subunit modulation of the $Ca_v1.2$ channel inactivation is associated with specific differences in voltage-gated molecular rearrangements between the NH_2-terminal regions of the α_{1C}- and β-subunits. This relationship was highlighted with reversible voltage-dependent differential corrected FRET measurements between the donor $(ECFP)_N$-β and acceptor $(EYFP)_N$-α_{1C} fluorophores of the functional Ca^{2+} channel complexes expressed in voltage-clamped living COS1 cells (Fig. 4). This method of patch clamp combined with FRET measurement was designed to determine the differences in relative proximity and/or angular orientation of the fluorescent FRET partners when the channel conformation is changed from the resting state (stabilized at −90 mV) to the inactivated ($\alpha_{1C,77}$) or sustained conducting ($\alpha_{1C,IS-IV}$) states, induced by depolarization to +20 mV (Table 1). The transition of the channels into each of these states before FRET imaging was controlled by voltage clamp and verified, in real time, by monitoring of the Ba^{2+} current during FRET measurements.

The reporter fluorophores were genetically fused to the NH_2-termini of the $\alpha_{1C,77}$- and $\alpha_{1C,IS-IV}$-subunits without considerable interference with the properties of the channels (Kepplinger et al., 2000; Kobrinsky et al., 2003). We find that the NH_2-terminal region is a convenient site for the attachment of GFP variants to the β-subunit. Earlier Wei et al. (2000) have described acceleration of the Ba^{2+} current inactivation imparted by the NH_2-terminal fusion of GFP to the β_{2a}-subunit cloned from the rat heart (Perez-Reyes et al., 1992). However, the rabbit β_2-subunit (Hullin et al., 1992) was $(ECFP)_N$-labeled in our work without substantial change

in the inactivation properties (see Fig. 4 *B*, *left traces*). Most important, the characteristic difference in modulation of the Ca^{2+} channel by the rabbit β_{1a}- and β_2-subunits was retained after the $(ECFP)_N$-labeling, as one can see, for example, from the comparison of the representative 1-s current traces in Fig. 4, *A* and *B*. The nature of this difference in terms of molecular dynamics of the α_{1C}- and β-subunits in a functional channel has been investigated here by differential state-dependent FRET microscopy.

Differential corrected FRET microscopy eliminates artifacts associated with the tagged orphan subunits and, by focusing on the relative changes in corrected FRET between the resting (−90 mV) and different inactivation states (+20 mV) of the channels, provides an estimate of the extent of voltage-gated intermolecular motion. We assume that the environment of the fluorophores may be structured by physical association of the subunits, and their segmental motions may not independently randomize the orientations (orientation factor $\kappa^2 \leq 2/3$) (Lakowicz, 1999). These assumptions generally complicate interpretation of the data in terms of translational distances between donor and acceptor, but appear to be physiologically relevant.

Differential corrected FRET microscopy did not reveal significant voltage-dependent changes in proximity to the plasma membrane of the $(ECFP)_N$-tags of β-subunits in the functional $\alpha_{1C,77}$ channel (Fig. 5). However, large voltage-dependent differences were observed in N_{FRET} between the N-terminal fluorophores of the β- and $\alpha_{1C,77}$-subunits (Table 1).

In the resting state of the channel, corrected FRET between the $(ECFP)_N$-labeled β_{1a}- or β_2-subunit and $(EYFP)_N$-$\alpha_{1C,77}$ was small (Table 1) and close to the detection limit of the method thus not permitting comparison between the $\alpha_{1C,77}/\beta_{1a}$ and $\alpha_{1C,77}/\beta_2$ channels. Inactivation of the $\alpha_{1C,77}/\beta_{1a}$ channel was accompanied by a substantial rearrangement between the NH_2-terminal regions of the β_{1a}- and $\alpha_{1C,77}$-subunits. The respective increase in corrected FRET between the donor $(ECFP)_N$-β_{1a} and acceptor $(EYFP)_N$-$\alpha_{1C,77}$ fluorophores (Fig. 4 *A*, *panel f*) may reflect differential β-subunit modulation, because it was not seen with the β_2-subunit (Table 1).

Lack of state-dependent FRET between the NH_2-terminal β_2 and $\alpha_{1C,77}$ fluorophores contrasts with strong state-dependent FRET in the $\alpha_{1C,77}/\beta_{1a}$ channel. There are essentially two explanations to this difference in terms of molecular rearrangements. One possibility suggests that state-dependent rearrangements between the NH_2-terminal fluorophores in the $\alpha_{1C,77}/\beta_2$ channel occur in a direction opposite to those observed in the $\alpha_{1C,77}/\beta_{1a}$ channel complex, e.g., further apart from the low-FRET resting arrangement and, thus, outside of the detection limits of the method. This might correspond, for example, to an increase in a linear distance between the NH_2-terminal fluorophores of the $\alpha_{1C,77}$- and β_2-subunits over 10 nm, and/or to perpendicular orientation approached by the ECFP/EYFP dipoles. The other possibility suggests that bulky β_2 might impede the voltage-gated mobility between the subunits as compared to β_{1a}. The FRET data (Table 1) don't allow one to discriminate between these two scenarios with sufficient confidence because the N_{FRET} values for the $\alpha_{1C,77}/\beta_2$ channel are small at both −90 and +20 mV. However, they indicate that the voltage-dependent rearrangement between the β_2 and $\alpha_{1C,77}$ fluorophores is fundamentally different from those between the β_{1a}- and $\alpha_{1C,77}$-subunits. This difference may be related to differential β-subunit modulation of inactivation, because both were eliminated by inhibition of the slow inactivation mechanism of the $\alpha_{1C,IS\text{-}IV}$ channel (Fig. 4, *D* and *E*). It was proposed that ADSI is crucial for a state-dependent folding of the pore-underlying polypeptide bundle associated with specific arrangement of the C-terminal Ca^{2+} sensors of inactivation (Soldatov, 2003). The β-subunit constitutes another component of that arrangement involved in AID binding and other interactions essential for slow inactivation. Robust state-dependent FRET between the $\alpha_{1C,IS\text{-}IV}$- and β-subunits NH_2-tails lacks β-subunit specificity probably because the mutation of ADSI causes desintegration of the bundle and eliminates physical constrains for the β-subunit movement (Fig. 6).

Molecular determinants of differential β-subunit modulation of inactivation

We found that voltage-gated rearrangements between the NH_2-terminals of the β- and $\alpha_{1C,77}$-subunits occur in a plane parallel to the plasma membrane (Fig. 6). Shistik et al. (1998) have proposed that β-subunits modulate the $Ca_v1.2$ channel by relieving an inhibitory control of the NH_2-terminus of α_{1C} over the activity of the channel. Lack of state-dependent FRET between the α_{1C} cytoplasmic NH_2-tail and the plasma membrane may be due to an impediment of the NH_2-tail voltage-gated conformational mobility by β-subunits that might generate a molecular signal for gating facilitation in a β-subunit specific manner.

The rabbit β_2-subunit studied in our work does not have NH_2-terminal cysteine sites of palmitoylation that may limit its voltage-gated mobility by anchoring to the plasma membrane (Chien et al., 1998; Qin et al., 1998; Gao et al., 1999; Restituito et al., 2000). As cytosolic proteins, β-subunits can't be subject to voltage-dependent rearrangements, which are apparently transduced to them via the AID locus of the linker between transmembrane segments IS6 and IIS1 of α_{1C}. Previously, Stotz and Zamponi (2001) proposed a role for the β-subunit-binding I-II linker of the α_1-subunit as a plug docking to segments IIS6 and IIIS6 in a ''hinged-lid'' inactivation mechanism. Among other structural factors, we find ADSI to be a crucial determinant. The role of β-subunits as modulators of slow voltage-dependent inactivation shown in this, and other reports (Sokolov et al., 2000) suggests a rationale for the model assuming that β-subunits differentially interfere with the slow inactivation mechanism. Experiments support this

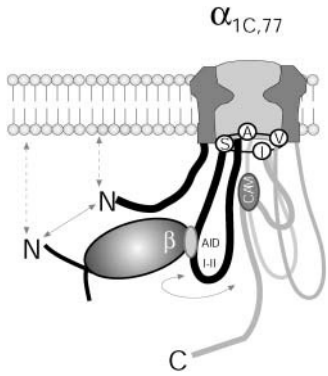

FIGURE 6 Hypothetical model of the voltage-gated molecular rearrangements of the NH_2-terminal regions of the Ca^{2+} channel $\alpha_{1C,77}$- and β-subunits. A β-subunit is shown bound via AID to the I-II loop of $\alpha_{1C,77}$. Four amino acids (Ser, Ala, Val, and Ile) of ADSI at the cytoplasmic ends of transmembrane segments S6 are indicated in a single-letter code in circles. The C-terminal tail (where CAM stands for tethered calmodulin) and other polypeptide bundle components, connected to the pore via ADSI, but not investigated in this work, are shown by shaded lines. We suggest that ADSI is crucial in communicating the voltage-dependent rearrangements in the pore to the AID locus. Shown are two types of rearrangements (*double-headed arrows*), associated with voltage-gated inactivation of the channel, that might affect relative proximity between the NH_2-terminals of the $\alpha_{1C,77}$- and β_{1a}-subunits without changing their proximity to the plasma membrane (*dashed arrows*). Such rearrangements are hindered in the case of the $\alpha_{1C,77}$- and β_2-subunits.

assumption and show that ADSI mutation uncouples the interaction of either β-subunit with the slow inactivation mechanism, equates, and probably facilitates the voltage-gated rearrangements between the NH_2-terminals of the β_{1a}- or β_2- and $\alpha_{1C,IS\text{-}IV}$-subunits.

In conclusion, we observed voltage-dependent rearrangements of NH_2-terminal regions of the α_{1C}- and β-subunits associated with differential β-subunit modulation of the channel inactivation. The approach developed here may complement crystallographic studies by providing characterization of the dynamic molecular changes associated with distinct functional states of ion channels in live cell.

We thank F. Hofmann (Munich, Germany) for the gift of plasmids coding for β_{1a}-, β_2-, and $\alpha_2\delta$-subunits, T. Balla for the PH-domain coding vector, C. Shi for assistance with oocyte recordings, A. Blatt for help with molecular biology, Sarah Bentil for help with image analysis, and D. E. Mager and Ira Josephson for critically reading the manuscript.

This work was supported in part by the National Institute on Aging Intramural Research Program (N.M.S.) and Austrian Science Foundation (P-15387 to C.R.).

REFERENCES

Baumgartner, W., K. Hohenthanner, G. F. Höfer, K. Groschner, and C. Romanin. 1997. Estimating the number of channels in patch-clamp recordings: application to kinetic analysis of multi-channel data from voltage-operated channel. *Biophys. J.* 72:1143–1152.

Berney, C., and G. Danuser. 2003. FRET or no FRET: a quantitative comparison. *Biophys. J.* 84:3992–4010.

Birnbaumer, L., N. Qin, R. Olcese, E. Tareilus, D. Platano, J. Costantin, and E. Stefani. 1998. Structures and functions of calcium channel β subunits. *J. Bioenerg. Biomembr.* 30:357–375.

Chang, F. C., and M. M. Hosey. 1988. Dihydropyridine and phenylalkylamine receptors associated with cardiac and skeletal muscle calcium channels are structurally different. *J. Biol. Chem.* 236:18929–18937.

Chien, A. J., T. Gao, E. Perez-Reyes, and M. M. Hosey. 1998. Membrane targeting of L-type calcium channels. Role of palmitoylation in the subcellular localization of the β_{2a} subunit. *J. Biol. Chem.* 273:23590–23597.

Colecraft, H. M., B. Alseikhan, S. X. Takahashi, D. Chaudhuri, S. Mittman, V. Yegnasubramanian, R. S. Alvania, D. C. Johns, E. Marban, and D. T. Yue. 2002. Novel functional properties of Ca^{2+} channel β subunits revealed by their expression in adult rat heart cells. *J. Physiol.* 541:435–452.

De Waard, M., and K. P. Campbell. 1995. Subunit regulation of the neuronal α_{1A} Ca^{2+}channel expressed in *Xenopus* oocytes. *J. Physiol.* 485:619–634.

De Waard, M., M. Pragnell, and K. P. Campbell. 1994. Ca^{2+} channel regulation by a conserved β subunit domain. *Neuron.* 13:495–503.

Erickson, M. G., H. Liang, M. X. Mori, and D. T. Yue. 2003. FRET two-hybrid mapping reveals function and location of L-type Ca^{2+} channel CaM preassociation. *Neuron.* 39:97–107.

Ferreira, G., J. Yi, E. Rios, and R. Shirokov. 1997. Ion-dependent inactivation of barium current through L-type calcium channels. *J. Gen. Physiol.* 109:449–461.

Gao, T., A. J. Chien, and M. M. Hosey. 1999. Complexes of the α_{1C} and β subunits generate the necessary signal for membrane targeting of class C L-type calcium channels. *J. Biol. Chem.* 274:2137–2144.

Gurnett, C. A., and K. P. Campbell. 1996. Transmembrane auxiliary subunits of voltage-dependent ion channels. *J. Biol. Chem.* 271:27975–27978.

Hummer, A., O. Delzeith, S. R. Gomez, R. L. Moreno, M. D. Mark, and S. Herlitze. 2003. Competitive and synergistic interactions of G protein β_2 and Ca^{2+} channel β_{1b} subunits with $Ca_v2.1$ channels, revealed by mammalian two-hybrid and fluorescence resonance energy transfer measurements. *J. Biol. Chem.* 278:49386–49400.

Hullin, R., I. F. Y. Khan, S. Wirtz, P. Mohacsi, G. Varadi, A. Schwartz, and S. Herzig. 2003. Cardiac L-type calcium channel beta-subunits expressed in human heart have differential effects on single channel characteristics. *J. Biol. Chem.* 278:21623–21630.

Hullin, R., D. Singer-Lahat, M. Freichel, M. Biel, N. Dascal, F. Hofmann, and V. Flockerzi. 1992. Calcium channel β subunit heterogeneity: Functional expression of cloned cDNA from heart, aorta and brain. *EMBO J.* 11:885–890.

Kepplinger, K. J. F., H. Kahr, G. Förstner, M. Sonnleitner, H. Schneider, T. Schmidt, K. Groschner, N. M. Soldatov, and C. Romanin. 2000. A sequence in the carboxy-terminus of the α_{1C} subunit important for targeting, conductance and open probability of L-type Ca^{2+} channels. *FEBS Lett.* 477:161–169.

Kobrinsky, E., E. Schwartz, D. R. Abernethy, and N. M. Soldatov. 2003. Voltage-gated mobility of the Ca^{2+} channel cytoplasmic tails and its regulatory role. *J. Biol. Chem.* 278:5021–5028.

Lakowicz, J. R. (1999). Principles of Fluorescence Spectroscopy. Kluwer Academic/Plenum Publishers, New York.

Meir, A., D. C. Bell, G. J. Stephens, K. M. Page, and A. C. Dolphin. 2000. Calcium channel β-subunit promotes voltage-dependent modulation of α_{1B} by $G_{\beta\gamma}$. *Biophys. J.* 79:731–746.

Mori, Y., T. Friedrich, M.-S. Kim, A. Mikami, J. Nakai, P. Ruth, E. Bosse, F. Hofmann, V. Flockerzi, T. Furuichi, K. Mikoshiba, K. Imoto, T. Tanabe, and S. Numa. 1991. Primary structure and functional expression from complementary DNA of a brain calcium channel. *Nature.* 350: 398–402.

Perez-Reyes, E., A. Castellano, H. S. Kim, P. Bertrand, E. Baggstrom, A. E. Lacerda, X. Wei, and L. Birnbaumer. 1992. Cloning and expression of a cardiac/brain β subunit of the L-type calcium channel. *J. Biol. Chem.* 267:1792–1797.

Pragnell, M., M. De Waard, Y. Mori, T. Tanabe, T. P. Snutch, and K. P. Campbell. 1994. Calcium channel β-subunit binds to a conserved motif in the I-II cytoplasmic linker of the α_1-subunit. *Nature*. 368:67–70.

Qin, N., D. Platano, R. Olcese, J. L. Costantin, E. Stefani, and L. Birnbaumer. 1998. Unique regulatory properties of the type 2a Ca^{2+} channel β subunit caused by palmitoylation. *Proc. Natl. Acad. Sci. USA*. 95:4690–4695.

Restituito, S., T. Cens, C. Barrere, S. Geib, S. Galas, M. De Waard, and P. Charnet. 2000. The β_{2a} subunit is a molecular groom for the Ca^{2+} channel inactivation gate. *J. Neurosci.* 20:9046–9052.

Schmid, R., K. Seydl, W. Baumgartner, K. Groschner, and C. Romanin. 1995. Trypsin increases availability and open probability of cardiac L-type Ca^{2+} channels without effecting inactivation induced by Ca^{2+}. *Biophys. J.* 69:1847–1857.

Shi, C., and N. M. Soldatov. 2002. Molecular determinants of voltage-dependent slow inactivation of the Ca^{2+} channel. *J. Biol. Chem.* 277: 6813–6821.

Shistik, E., T. Ivanina, Y. Blumenstein, and N. Dascal. 1998. Crucial role of N terminus in function of cardiac L-type Ca^{2+} channel and its modulation by protein kinase C. *J. Biol. Chem.* 273:17901–17909.

Singer, D., M. Biel, I. Lotan, V. Flockerzi, F. Hofmann, and N. Dascal. 1991. The roles of the subunits in the function of the calcium channel. *Science*. 253:1553–1557.

Sokolov, S., R. G. Wei, E. N. Timin, and S. Hering. 2000. Modulation of slow inactivation in class A Ca^{2+} channels by β-subunits. *J. Physiol.* 527:445–454.

Soldatov, N. M. 2003. Ca^{2+} channel moving tail: link between Ca^{2+}-induced inactivation and Ca^{2+} signal transduction. *Trends Pharmacol. Sci.* 24:167–171.

Soldatov, N. M., A. Bouron, and H. Reuter. 1995. Different voltage-dependent inhibition by dihydropyridines of human Ca^{2+} channel splice variants. *J. Biol. Chem.* 270:10540–10543.

Soldatov, N. M., M. Oz, K. A. O'Brien, D. R. Abernethy, and M. Morad. 1998. Molecular determinants of L-type Ca^{2+} channel inactivation. Segment exchange analysis of the carboxyl-terminal cytoplasmic motif encoded by exons 40–42 of the human α_{1C} subunit gene. *J. Biol. Chem.* 273:957–963.

Soldatov, N. M., S. Zhenochin, B. AlBanna, D. R. Abernethy, and M. Morad. 2000. New molecular determinant for inactivation of the human L-type α_{1C} Ca^{2+} channel. *J. Membr. Biol.* 177:129–135.

Soldatov, N. M., R. D. Zühlke, A. Bouron, and H. Reuter. 1997. Molecular structures involved in L-type calcium channel inactivation. Role of the carboxyl-terminal region encoded by exons 40–42 in α_{1C} subunit in the kinetics and Ca^{2+} dependence of inactivation. *J. Biol. Chem.* 272: 3560–3566.

Stotz, S. C., and G. W. Zamponi. 2001. Structural determinants of fast inactivation of high voltage-activated Ca^{2+} channels. *Trends Neurosci.* 24:176–182.

Takahashi, S. X., S. Mittman, and H. M. Colecraft. 2003. Distinctive modulatory effects of five human auxiliary β_2-subunit splice variants on L-type calcium channel gating. *Biophys. J.* 84:3007–3021.

Tour, O., R. M. Meijer, D. A. Zacharias, S. R. Adams, and R. W. Tsien. 2003. Genetically targeted chromophore-assisted light inactivation. *Nat. Biotechnol.* 21:1505–1508.

van der Wal, J., R. Habets, P. Varnai, T. Balla, and K. Jalink. 2001. Monitoring agonist-induced phospholipase C activation in live cells by fluorescence resonance energy transfer. *J. Biol. Chem.* 276:15337–15344.

Wei, S.-K., H. M. Colecraft, C. D. DeMaria, B. Z. Peterson, R. Zhang, T. A. Kohout, T. B. Rogers, and D. T. Yue. 2000. Ca^{2+} channel modulation by recombinant auxiliary β subunits expressed in young adult heart cells. *Circ. Res.* 86:175–184.

Xia, Z., and Y. Liu. 2001. Reliable and global measurement of fluorescence resonance energy transfer using fluorescence microscopes. *Biophys. J.* 81:2395–2402.

Yamaguchi, H., M. Hara, M. Strobeck, K. Fukasawa, A. Schwartz, and G. Varadi. 1998. Multiple modulation pathways of calcium channel activity by a β subunit. Direct evidence of β subunit participation in membrane trafficking of the α_{1C} subunit. *J. Biol. Chem.* 273:19348–19356.